Contents lists available at ScienceDirect

Composites Part C: Open Access

Measurement of microfibril angle in plant fibres: Comparison between X-ray diffraction, second harmonic generation and transmission ellipsometry microscopies

Emmanuelle Richely [a], Ali Zarei [b], Alessia Melelli [c], Dhanesh Kattipparambil Rajan [b], Jason Govilas [d], Xavier Gabrion [d], Cédric Clévy [d], David Legland [a,e], Javier Perez [f], Sofiane Guessasma [a], Vincent Placet [d], Pasi Kallio [b], Johnny Beaugrand [a,*]

[a] *INRAE, UR1268 BIA Biopolymères Interactions Assemblages, Nantes, France*
[b] *Faculty of Medicine and Health Technology, Tampere University, Finland*
[c] *Synchrotron SOLEIL, DISCO-ANATOMIX beamlines, Gif-sur-Yvette, France*
[d] *University of Franche-Comté, FEMTO-ST Institute, Besançon, France*
[e] *INRAE, PROBE Research Infrastructure, BIBS Facility, Nantes, France*
[f] *Synchrotron SOLEIL, Heliobio team, SWING beamline, Gif-sur-Yvette, France*

ARTICLE INFO

ABSTRACT

The orientation of cellulose microfibrils within plant fibres is one of the main factors influencing their mechanical properties. As plant fibres are more and more used as reinforcement for agro-composites, their mechanical properties have a strong influence on the final composite properties. It is, therefore, of interest to obtain reliable information about the microfibril angle (MFA) to better support the choice of fibres depending on the product requirements. In the present study, the reliability and specificities of three non-destructive methods that allow analysis on the same fibre glued on a holder; X-ray diffraction (XRD), second harmonic generation (SHG) and transmission ellipsometry (TE) microscopy; are investigated. Three types of plant fibres, with both low (nettle), and high (cotton, sisal) MFA values, are compared and their geometry and biochemical composition are characterised. The results obtained on the same fibre confirm that MFA analysis remains tedious and that despite their limitations, the methods are complementary depending on the information requested. Indeed, SHG is recommended for direct, qualitative and plane-selective mapping of heterogeneities in macrofibril orientations at various depths. However, reliable quantitative results with SHG depend on the initial image quality and could benefit from further image processing refinement. On the contrary, XRD and TE measure MFAs over the entire fibre thickness and provide variations along the fibres if a sufficient optical/spatial resolution is reached. Regarding the characterization of intrinsic defects in plant fibres, both SHG and TE suffer from uncertainties induced by the disorganization of the microfibril network and the lack of symmetry between the front and back fibre walls. Finally, all techniques prove to be dependant on the initial fibre alignment and geometry (i.e. twisting, double fibre configuration or form factor) which vary along the fibre length and should be carefully taken into account.

1. Introduction

The interest for plant fibres as alternatives to synthetic fibres has been growing in the past decades [1], in a context of intensifying environmental concern. Such materials directly shaped by Nature often embody a complex structure, and a better knowledge of their structure-property relationship is required to develop further their use in composite applications. It is especially the case for the cellulose microfibril orientation, which is one of the main ultrastructural features governing the stiffness of the plant fibres [2,3].

Indeed, plant fibres are multilayer composite arrangements composed of cellulose microfibrils surrounded by amorphous polysaccharides such as hemicelluloses, lignin and pectins. The crystalline cellulose microfibrils act as a reinforcement in the cell wall, are

---

* Corresponding author.
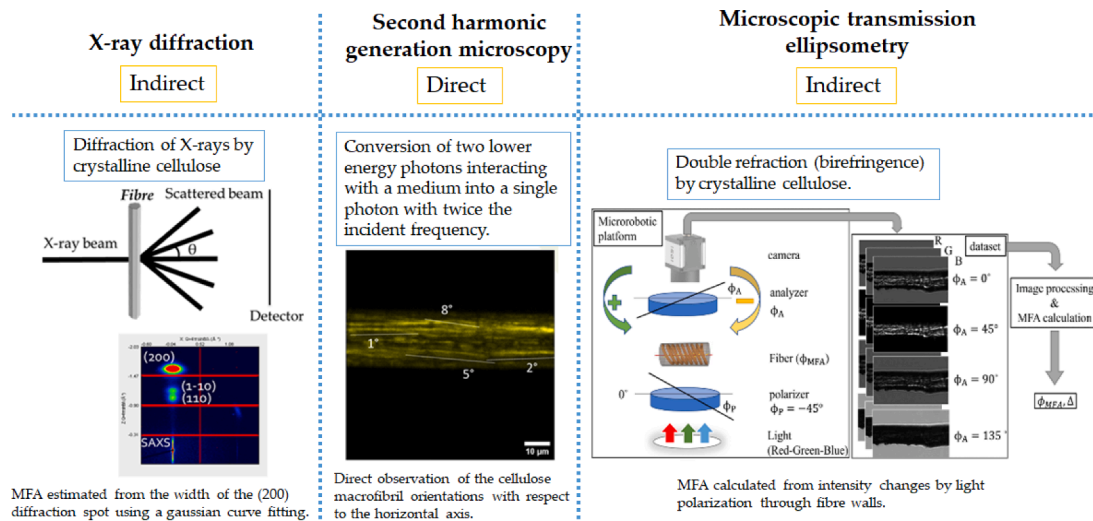*E-mail address:* johnny.beaugrand@inrae.fr (J. Beaugrand).

Fig. 1. Outline of the principle of the methods used in the present study to measure the microfibril angle of sisal, nettle and cotton fibres.
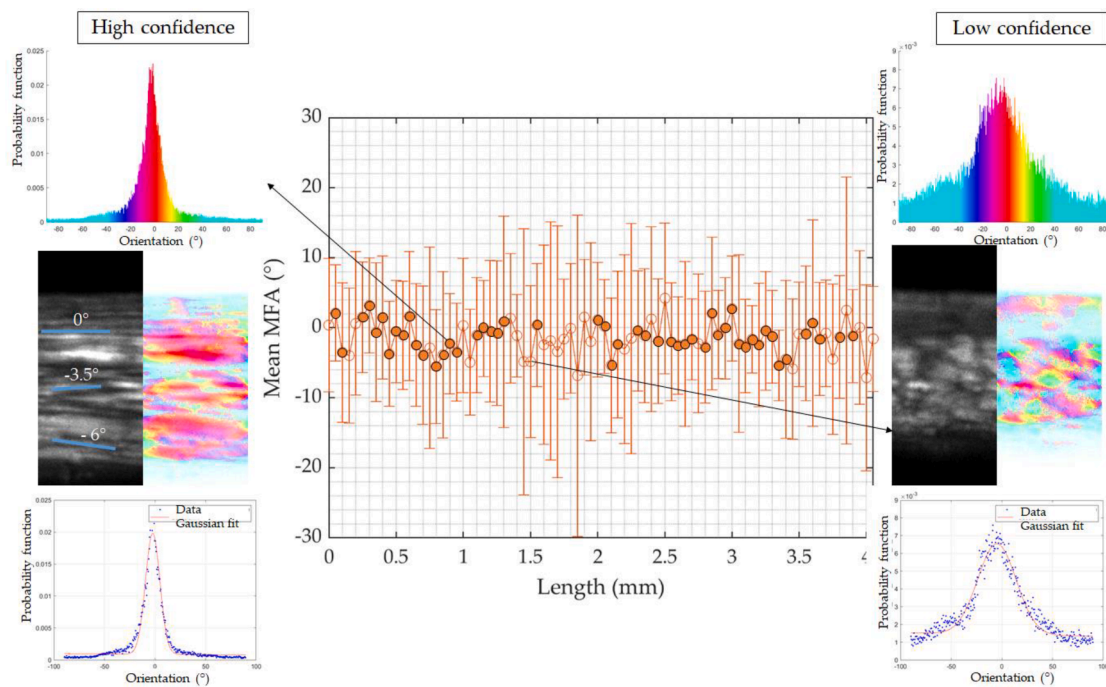

Fig. 2. Mean MFA and standard deviation obtained along nettle fibre N1 by SHG using a Gaussian curve fitting. The filled circles represent data with high confidence. Two examples of initial images, MFA mappings and related histogram with high and low confidence are displayed to the left and right, respectively.

backboned with semi-crystalline parts, and are orientated with a particular angle with respect to the fibre axis, which is called the microfibril angle (MFA). These microfibrils (3-4 nm in diameter for wood) aggregate into macrofibrils (up to 60 nm in diameter), which is often the scale at which direct observations are made [4]. The respective polysaccharide contents, cellulose crystallinity and orientation, sublayer arrangement and organization as well as porosity content differ from one plant fibre to another, linked to their role within the plants [5]. Moreover, the macrofibril network might be disrupted at some specific areas along the fibres. These disrupted areas are called defects, dislocations or kink bands [6]. Several recent articles have tackled the link between the defect formation and the mechanical extraction of the fibres [7–9], but a better characterization and understanding of their effect on the mechanical properties remain of interest to further accelerate the use of plant fibres in structural applications.

Several direct methods involving microfibril exposure followed by imaging are described in the literature to estimate the MFA within plant fibres, including wood [3]. Staining methods and microscopy observations were already described during the first half of the 20th century [10,11]. In the case of wood, fibre sonication in solutions of cobalt and copper have been reported [12]. Moreover, fibre peeling followed by scanning electron microscopy (SEM) imaging has also been used to determine the MFA of different sublayers [13], as well as preparation of thin fibre sections for transmission electron microscopy [14,15]. However, these techniques are destructive and require very rigorous and time-consuming sample preparations, which adversely affect the cell wall organisation. Cellulose is a non-centrosymmetric molecule and has a capability to produce Second Harmonic Generation (SHG) signal. In plant research, cellulose properties have been already investigated using SHG imaging including an emerging method known as
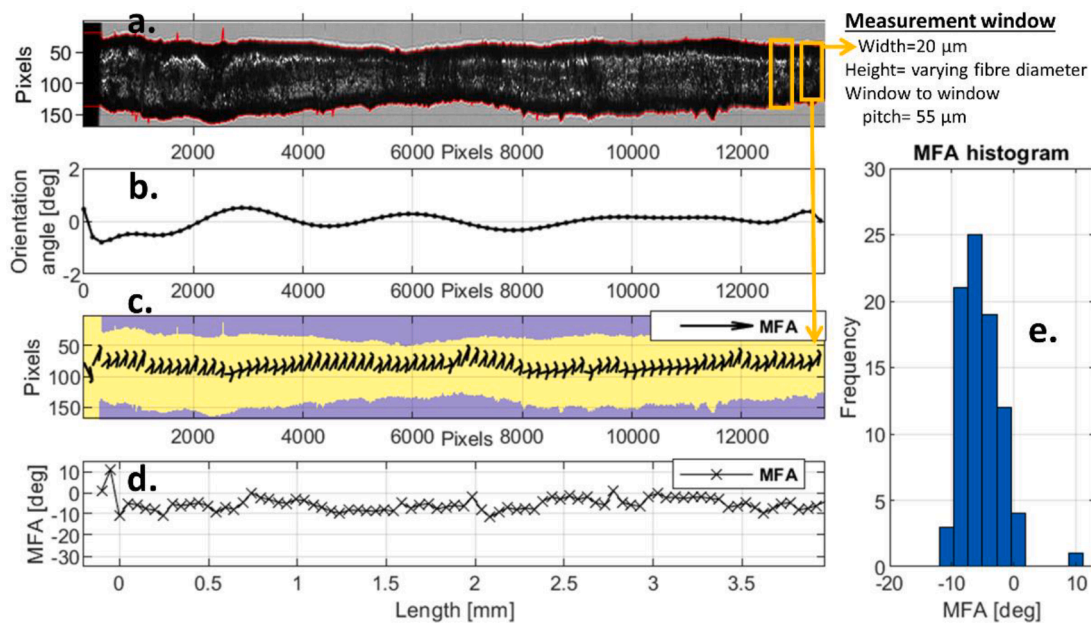
Fig. 3. Mean MFA computed along nettle fibre N1 using Transmission Ellipsometry. (a) Fibre image (the whole length squeezed for demonstration) showing non-uniformity in diameter. along the length of the fibre. The scanning window width was set to 20 μm (two example windows are shown in yellow rectangles) for XRD comparable mean MFA values, but a varying window height was opted to accommodate variations in fibre diameter along the length. (b) Measured fibre orientation angles along the length of the fibre showing deviation of the fibre axis from a horizontal alignment. (c-d) Estimated MFAs as quiver vector plots and a line plot. (e) The histogram of all MFAs where the distribution could indicate several possible ultrastructural and defects causes.
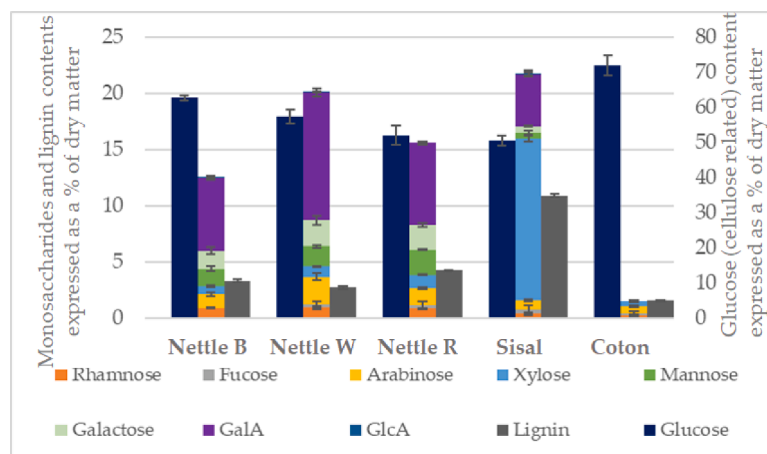

Fig. 4. Analysis of lignin, glucose (related to cellulose) and non-glucosidic monosaccharide content of nettle, sisal and cotton fibres used in this study.

Polarization-resolved Second Harmonic Generation microscopy (P-SHG). This latter method provides direct observation of the cellulose macrofibrils at different depth planes [16,17]

X-ray diffraction is a popular indirect method to measure the MFA of plant fibres, with several existing procedures for interpretation of diffraction patterns [18,19]. Laboratory devices enable the measurement of the MFA from technical fibres (i.e. bundles of unitary fibres), but experience uncertainties linked to the strong assumption of perfect alignment of the fibres within a bundle. Additionally, only a mean lateral MFA can be estimated throughout the bundles. To reach the unitary fibre scale, synchrotron radiation is required [20,21].

Another indirect method, easier to implement in laboratories, is polarised light microscopy, which requires particular fibre preparation to keep just one pair of opposite cell walls [22,23]. The same drawback of altering the fibre structure is shared with confocal fluorescence microscopy, which requires the use of specific fluorescent dyes [18,24]. On the contrary, transmission ellipsometry (TE) microscopy, based on the birefringence capacity of crystalline cellulose microfibrils, gives an estimation of MFA without fibre pre-treatment [25]. Heterogeneous MFA values along a hemp fibre has been studied by polarised Raman microspectroscopy [26].

Each technique mentioned in Table 1 has its advantages and limitations. Although a few authors have compared the MFA obtained by XRD and microscopy techniques, there is still a lack of stringent comparison of reliability, repeatability and robustness amongst the most promising non-destructive ones. In this context, this scientific investigation aims at obtaining reliable, qualitative and quantitative MFA information using three complementary techniques: the well-established X-ray diffraction (XRD) using a Synchrotron source and two in-lab methods; polarized second harmonic generation microscopy (SHG) and microscopic transmission ellipsometry (TE) (Fig. 1). To study reliability, repeatability, and robustness of the three methods, three different plant fibres with high (sisal and cotton) and low (nettle) MFA values were chosen. To allow easier manipulation and reproducible
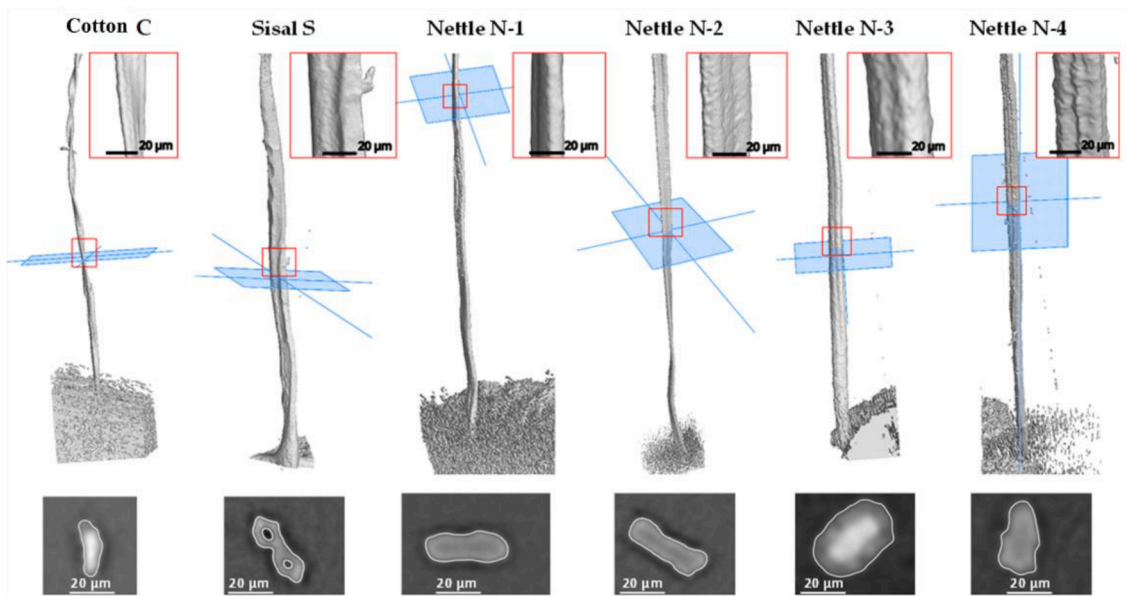
Fig. 5. 3D views (top) of one extremity of each plant fibre obtained from X-ray microtomography for a resolution of 0.45 μm, and related cross-sectional views (bottom).

Fig. 6. Mean MFA (a) and absolute mean MFA (e) obtained along a nettle fibre N1 by TE, SHG and XRD. Regarding SHG, the filled circles represent data with high confidence. In addition, bright light (b) and polarized light (c) images obtained by optical microscopy are displayed above the SHG mapping (d).
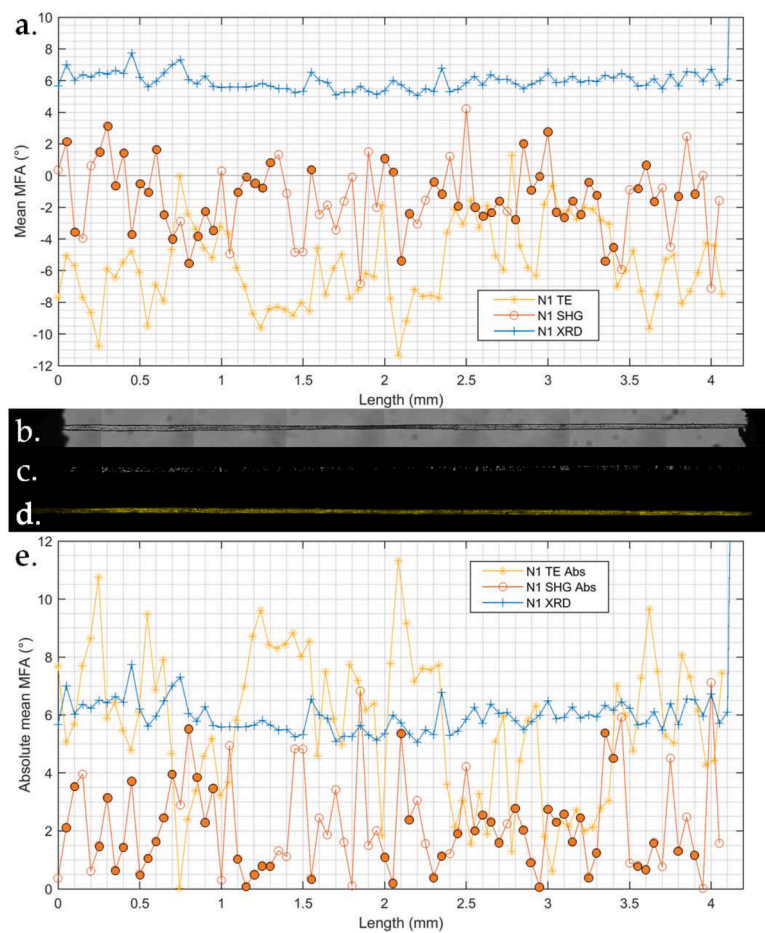
Fig. 7. Mean MFA (a) and absolute mean MFA (e) obtained along a nettle fibre N2 by TE, SHG and XRD. Regarding SHG, the filled circles represent data with high confidence. In addition, bright light (b) and polarized light (c) images obtained by optical micr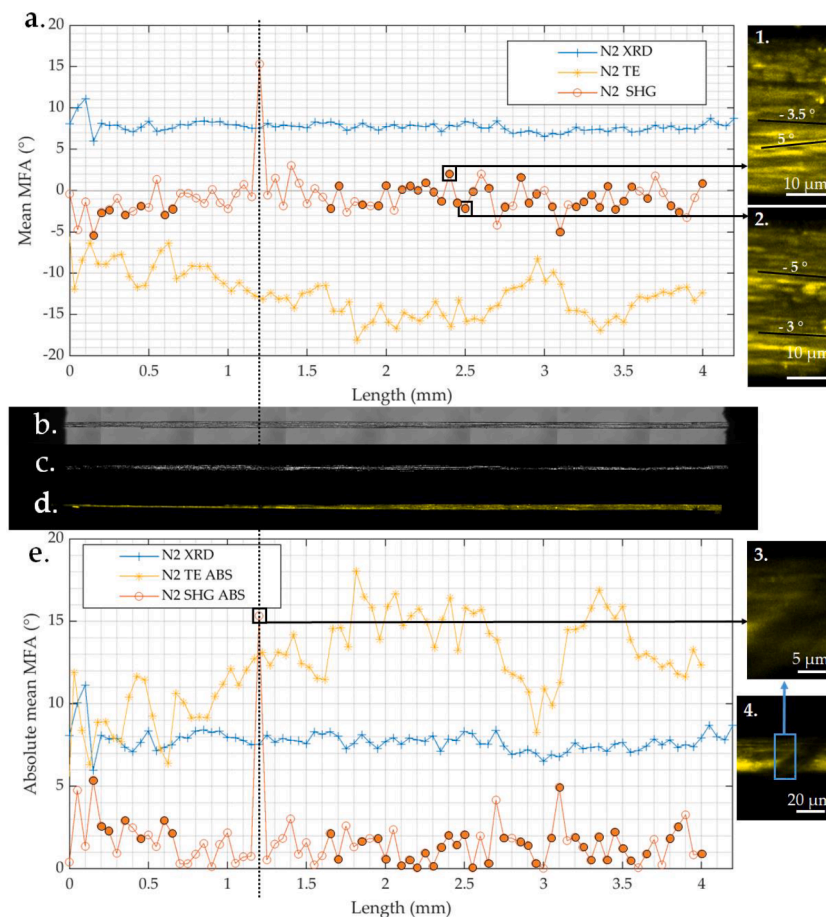oscopy are displayed above the SHG mapping (d). Magnified views of SHG along the fibre are also presented to the right (1 to 4).

testing, fibres were glued onto paper frames. The sensitivity and measurement range of each technique were assessed on the same fibre specimens.

2. Materials and methods

2.1. Materials

Stinging nettle (*Urtica dioïca*), sisal (*Agave sisalana*) and cotton (*Gossypium* sp.*)* fibres were provided for the study. Regarding the nettle fibres, the University of Bremen provided three types to compare: stinging nettle of Roville clone harvested in Doncières, France in July 2020 (N-R), of B13 clone harvested in Potsdam, Germany in October 2020 (N-B) and wild nettle found growing in a park in Bremen, Germany in 2019 (N-W). The sisal fibres were provided by PUC-Rio, Brazil and cultivated in Valente – Bahia (North of Brazil) by the company APAEB. Cotton trichomes issued from the genotype G3 BRS 293 were cultivated in Ntarla, Mali, in 2017.

The unitary fibres from all plants were extracted manually with tweezers and glued onto the paper frames for easier handling. The scanning length was limited by the maximum window allowed by the XRD device and chosen according to the length of the fibres, i.e. 4 mm for nettle and cotton and 1 mm for sisal. Initial microscopy images of each fibre were acquired using a microscope (Leitz DMRB, Leica Microsystems, Nanterre, France) equipped with a Hamamatsu digital camera (C11440 ORCA-Flash4.0 LT) and an x-y motorised stage (Marzhauser). Images were acquired with an optical objective x20 (pixel size: 328 nm) under both bright light and linearly polarised light; the

latter revealing the defects along the fibres which appear as bright areas [27]. The different unitary fibres scanned are summarized in Table 2. The complementary experiments were made in the following order: XRD, followed by TE and SHG, and X-ray microtomography.

2.2. Biochemical analysis

For all biochemical analysis, the first step of homogenization was performed by cryogrinding (SPEX 6700 freezer Mill) approximately 2 g of raw bundles into a powder. Three independent assays were performed for each fibre sample. The chemicals were laboratory grade from Sigma Aldrich. Regarding the analysis of monosaccharide, the powdered samples (approximately 5 mg per trial) were subjected to a pre-hydrolysis in 12 M H_2SO_4 during two hours at 25 °C [28]. It was followed by a hydrolysis step in 1.5 M H_2SO_4 during two hours at 100 °C [28], after addition of inositol used as an internal standard [29]. The alditol acetate derivatives of the neutral sugars [30] were analysed by gas phase chromatography (Perkin Elmer, Clarus 580, Shelton, CT, USA) equipped with an DB 225 capillary column (J&W Scientific, Folsorn, CA, USA) at 205 °C, with H_2 as the carrier gas and a flame ionisation detector. Standard sugar solutions of known concentrations were used as calibration. Galacturonic acid (GalA) and glucuronic acid (GlcA) were merged as uronic acids and determined by the m-hydroxybiphenyl method [31], a colorimetric quantification. Lignin content was quantified by spectrophotometry following the acetyl-bromid method [32]. The mean values expressed as the percentage of dry matter were reported as analysis results.
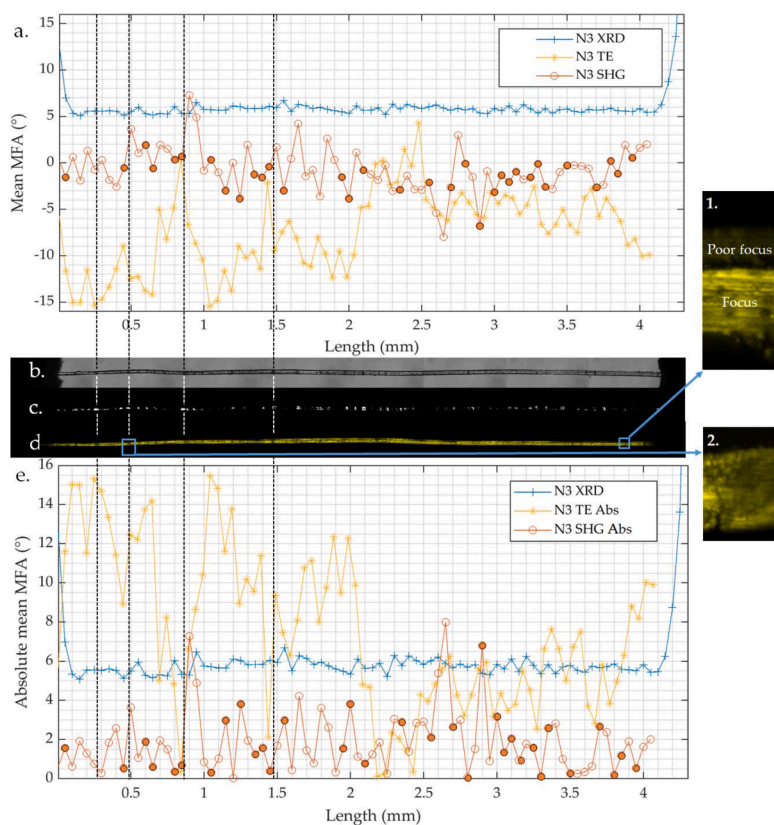
Fig. 8. Mean MFA (a) and absolute (Abs) mean MFA (e) obtained along a nettle fibre N3 by TE, SHG and XRD. Regarding SHG, the filled circles represent data with high confidence. In addition, bright light (b) and polarized light (c) images obtained by optical microscopy are displayed above the SHG mapping (d). Magnified views of SHG along the fibre are also presented to the right, highlighting zones of poor focus (1.) possibly linked to the geometry of the fibre and a darker zone corresponding to a defect (2.).
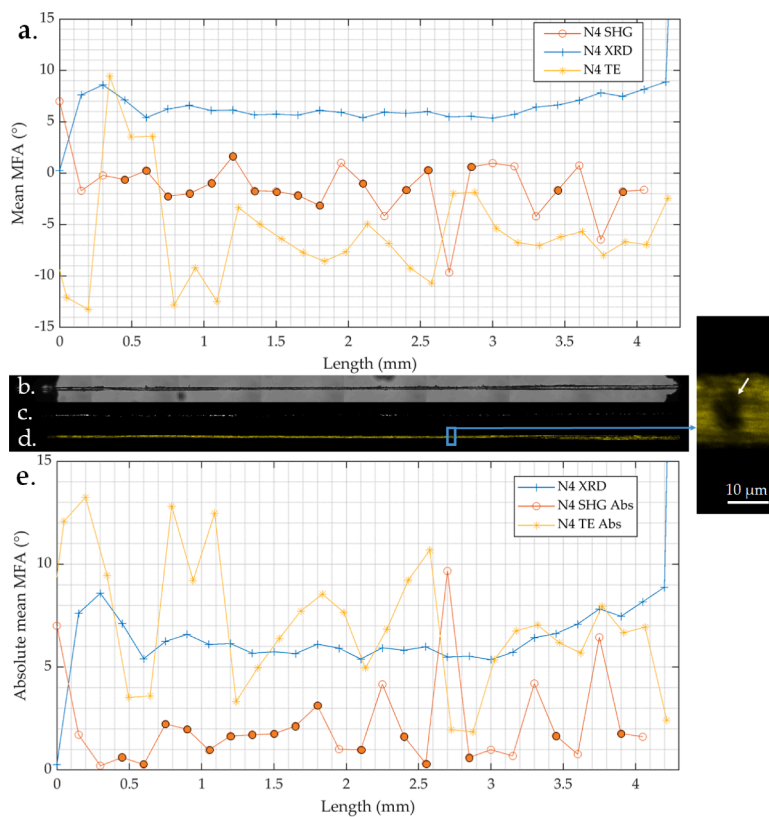
Fig. 9. Mean MFA (a) and absolute mean MFA (e) obtained along a nettle fibre N4 by TE, SHG and XRD. Regarding SHG, the filled circles represent data with higher confidence. In addition, bright light (b) and polarized light (c) images obtained by optical microscopy are displayed above the SHG mapping (d). A magnified view of SHG along the fibre is also presented to the right, highlighting a dark area likely induced by surface impurities.
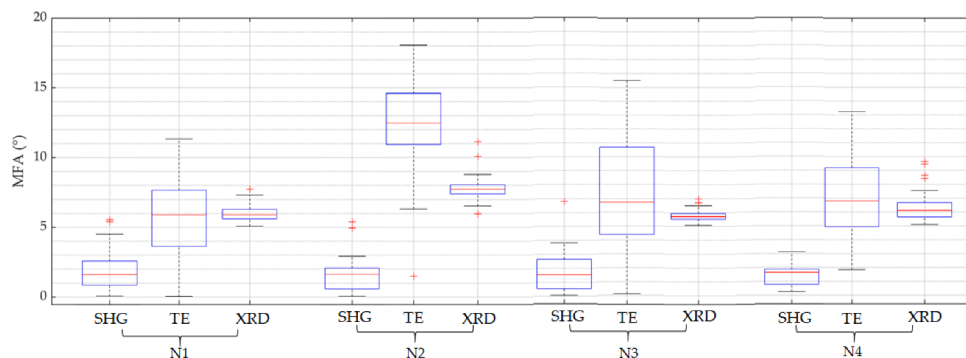
Fig. 10. Boxplots of the MFA obtained by SHG, TE and XRD along nettle fibres N1 to N4. The bottom and top of the box indicate the 25th and 75th percentiles, respectively, and the central red line indicates the median. The outliers are plotted with a symbol '+' and the whiskers extend to the most extreme data points not considering outliers. Those outliers were determined using the boxplot function of MATLAB, as data points that are more than 1.5*interquartile range from the median.
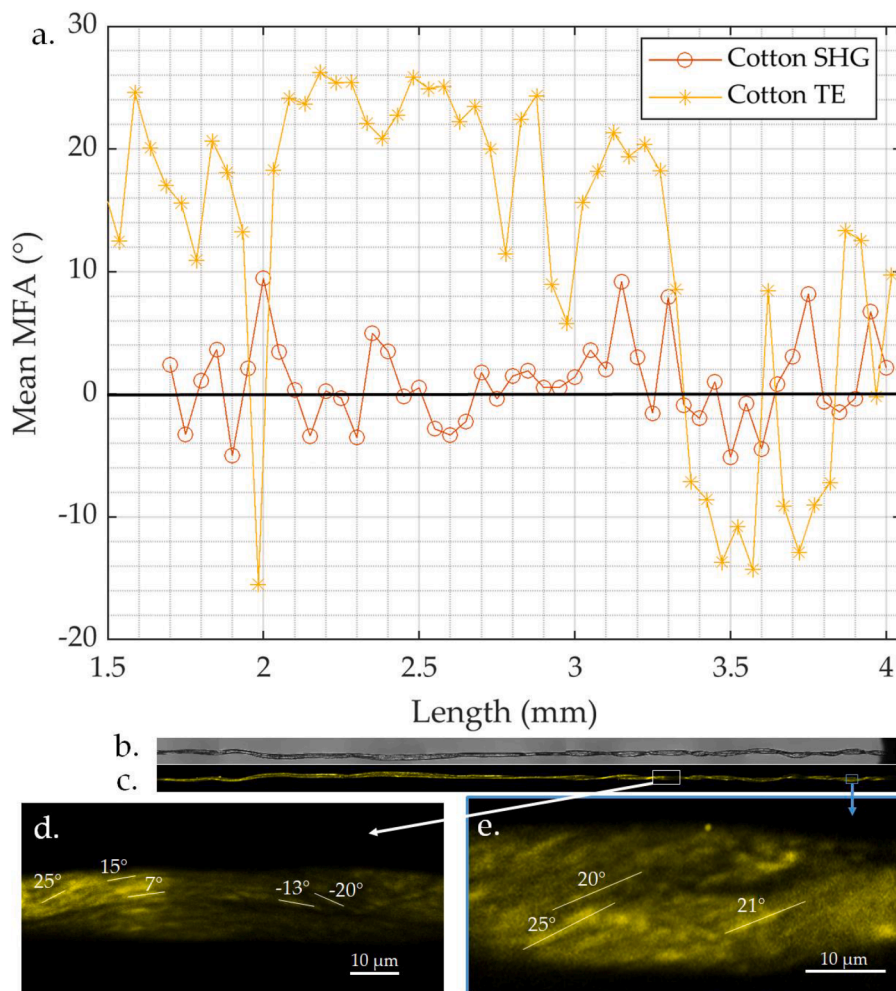

Fig. 11. a) Mean MFA and standard deviation obtained along a cotton fibre by TE and SHG, with b) bright light image obtained by optical microscopy and c) SHG image highlighting the twists along the cotton fibre. Two magnified views along the SHG image are presented in d) and e) with examples of MFA values obtained by direct observation of the macrofibrils.

2.3. X-ray microtomography

X-ray microtomography was performed on an EasyTom tomograph (RX Solutions, Chavanod, France). The fibres were glued vertically onto the paper frame to avoid movement during acquisition. The sample holder was mounted on a rotating table to allow a rotation of 360° The X-ray source Hamamatsu Open Type Microfocus L10711 was operated with an electron current of 84 µA and a tube voltage of 60 kV. The X-ray transmission images were acquired using a CCD camera with 2016 × 1344 pixels. The exposure time and the average frame were fixed at two

seconds and six images respectively; and 416 images per revolution were acquired. The entire volume was reconstructed at a full resolution with a voxel size of 0.45 µm corresponding to a field of view of 0.9×0.6 mm^2, using filtered back-projection. For all fibres, a stack tomography was necessary to acquire the entire length of the fibre, which is different for each fibre. The total length, the number of turns and images, and the duration of tomography are summarized for each fibre in Table 3. The data analysis was performed using VG StudioMax software. The analysis of the grey levels was achieved using a threshold to separate the material from the air and access the geometry of the fibre.
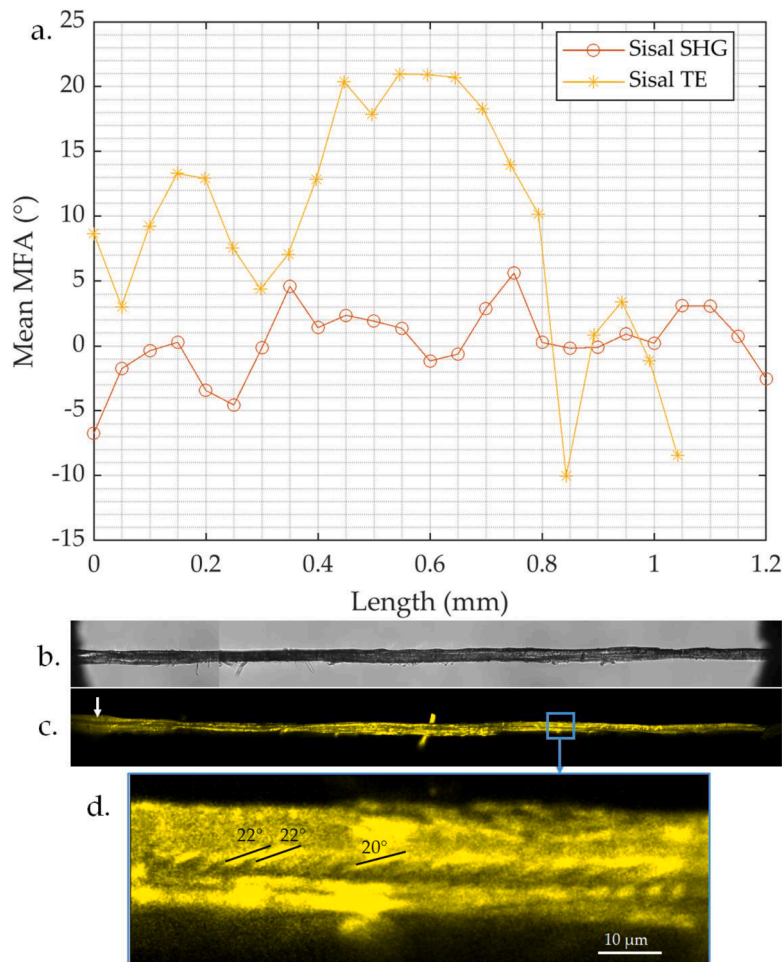
Fig. 12. (a): Mean MFA and standard deviation obtained along a sisal fibre by TE and SHG, with b) bright light image obtained by optical microscopy and c) SHG image along the sisal fibre, with a white arrow highlighting the fibre lumen. A magnified view along the SHG image is presented in d) with examples of MFA values obtained manually.

2.4. X-ray diffraction

X-ray diffraction was performed on the SWING beamline of SOLEIL Synchrotron (Gif-sur-Yvette, France), with an X-ray beam energy of 15 keV and an X-ray beam length of 250×20 μm. The relative humidity (RH) and temperature of the testing chamber were recorded as $30 \pm 5\%$ RH and 22 ± 2 °C, respectively. A CCD detector of 1032×1088 pixels (77.4×81.6 mm) was placed 520 mm apart from the sample, leading to a quarter of the diffraction pattern, with q values up to 2.03 $Å^{-1}$. The sample holder was placed on two translating tables, allowing 1 μm precision on the displacements in the horizontal and vertical directions. Several measurements were taken along the entire fibre lengths, and the spacing between the measurements is specified in Table 2 for each fibre. When needed, jaw displacements of 10 μm were applied to each fibre until reaching an initial force of 0.01 N to ensure a straight fibre. Data processing was performed using Foxtrot software developed at Synchrotron SOLEIL. The diffraction spot corresponding to the (200) planes was selected for the MFA estimation, following the method described in a previous study [33]. The first radial integration of the intensity was conducted on the masked diffraction pattern, with a Gaussian curve fitting to estimate the optimal diffusion vector Q_0 corresponding to the maximum intensity of the (200) plane. At this particular Q_0, the second integration of the azimuthal profile was performed, resulting in a standard deviation obtained by a Gaussian curve fitting. The standard deviation is related to the Half Width at Half Maximum (HWHM) and to the MFA through the following equation:

$$MFA(°) = HWHM \approx 1.178 * \sigma \qquad (1)$$

where σ corresponds to the gaussian Half Width at Half Maximum. As mentioned in the previous work conducted by the team [33], this simple method does not take into account the geometry of the fibre, nor the possible initial fibre tilt, which might influence the results. However, it is sufficient to highlight the variations along the fibres.

2.3. Second harmonic generation microscopy

SHG measurements were performed on a multiphoton Nikon A1 MP and a microscope (NIKON, France) equipped with a long working distance (LWD) 16x (NA 0.80) water immersion objective (NIKON, France), a tuneable Mai Tai XF mode-5 locked Ti:sapphire femtosecond laser (SPECTRA PHYSICS, France) and a half-wave plate (MKS-Newport, USA) placed in front of the laser excitation beam. At an excitation wavelength of 810 nm, the average laser power was 1.5 W. In order to avoid damage on the fibres and photobleaching, only 5% of the power was used. However, it should be noted that even under optimised conditions, SHG can be destructive if the fibre is particularly weak in localized areas or if the surface is rich in cortical residues and remnants of the middle lamella. Both the backward and forward signals were collected with three bandpass filters at 460/60 nm (autofluorescence), 550/88 nm (autofluorescence) and 406/15 nm (SHG signal) but only the forward SHG channel was selected to calculate the angle of macrofibrils. GaAsP NDD (gallium arsenide non-descanned) detectors were used. The

Table 1

Summary of the methods used to measure the microfibril angle.

Method		Destructive or bias of preparation	Advantages	Limits
Optical or scanning electron microscopy with pre-treatment	Staining [9]	Yes	Direct	Tedious
	Fibre sonication [11]	Yes	Direct	- Tedious - Immersion that can alter the initial MFA
	Fibre peeling [12]	Yes	Direct	- Tedious - Mechanical constraint that could bias the MFA
Polarized light microscopy	Mercury impregnation [17]	Yes	–	- Indirect - Tedious - Not applicable to fibres with collapsed or distorted lumen
	Initial longitudinal cutting [55]	Yes	–	- Indirect - Tedious
Confocal fluorescence microscopy	Fluorescent dyes	Yes	Fast	- Indirect -Tedious
Polarized FTIR microspectroscopy [22],[55],		No	Other components, like lignin and hemicelluloses, can be analysed at the same time	- Indirect - Map of small areas - Slow, tedious data processing - Estimation of a range of MFAs but no possible histograms - No information on local changes of MFAs
Polarised Raman microspectroscopy [23]		No	–	- Indirect - Map of small areas - Slow, tedious data processing
Transmission electron microscopy on thin sections [13, 14]		Yes	Direct	- Tedious - Lack of reference axis
Polarized second harmonic generation microscopy [15]		No, under optimised setting	- Direct - Relatively fast - -Plane selective	- Perfect alignment of the fibre required - Well-ordered, crystalline structure necessary to obtain signal - Semi-quantitative information depending on the quality of the signal; difficult image processing
X-ray diffraction [12,18,26,56]		No under optimised doses	Fast, can explore large areas	- Indirect - Synchrotron source needed to reach unitary fibre scale - Perfect alignment of the fibre required - Numerous data processing possibilities
Microscopic transmission ellipsometry [20]		No	Fast, can explore large areas	- Indirect -Perfect alignment of the fibre required

Table 2

List of samples used in the present study, together with their origin, diameter obtained by optical microscopy and techniques performed. The spacing between XRD measurements along the fibres is also specified. *X* : measurement done; - : attempted, but unsuccessful.

Type	Name	Diameter (µm)	SHG	XRD	TE
Nettle N-R fibres	N-1	32.9 ± 6.4	X	50 µm	X
	N-2	38.5 ± 0.5	X	50 µm	X
Nettle N-B fibres	N-3	32.9 ± 3.7	X	50 µm	X
Nettle N-W fibres	N-4	25.1 ± 4.9	X	150 µm	X
Cotton fibres	C	–	X	–	X
Sisal S-B fibres	S	20.1 ± 2.1	X	–	X

Table 3

Nomenclature, total length, number of turns and duration of tomography, for each tested fibre.

Type	Name	Length (mm)	Number of turns	Number of images	Time (h)
Nettle N-R fibres	N-1	1.4	5	2080	7.5
	N-2	3	8	3328	12
Nettle N-B fibre	N-3	4	8	3328	12
Nettle N-W fibre	N-4	2.7	7	2912	10.5
Cotton fibre	C	1.3	4	1664	6
Sisal S-B fibre	S	1.1	3	1248	4.5

scan line average was set to 16, the scan velocity was fixed at 0.5 (fps), and the scan size was 512×512 pixels. Several consecutive images were taken along the fibre by using a digital zoom of 10x (image of 80.04 × 80.04 µm, pixel size of 0.16 µm) with a step of 55 µm between them in order to reconstruct the entire fibre (4 mm for cotton and nettle and 1 mm for sisal). As information is acquired on a single observation plane

with SHG, the thickest layer S2 was chosen for each data acquisition. Before each acquisition, the half-wave plate was set parallel to the nettle fibre axis or at 30° for cotton and sisal, following Melelli et al. [16]. The images were taken with fibres in a dry state. The addition of water can improve the SHG signal. However, it was not preferable in the present study since all the other MFA measurements methods are performed

Table 4

Methodological comparison of sources of uncertainty in the XRD, SHG and TE techniques.

Sources of uncertainty	XRD	SHG	TE
Fibre geometry	Influence of fibre geometry not considered with the current processing method	Difficult observation for thinner cell walls	Assumption of symmetry between the front and back walls
Twist	Induces uncertainties	Induces uncertainties	Induces uncertainties
Sublayers	Contribution of all sublayers	Single plane visible (unless twists)	Contribution of all sublayers
Fibre misalignment	Needs to be corrected	Needs to be corrected	Needs to be corrected
Bundles increasing the uncertainties	Yes, averaged MFA depending on the beam size	Not necessary, depending on the bundle configuration	Yes, depending on the bundle configuration
Influence of fibre surface impurities	Negligible if non-crystalline structure	Yes, might create dark areas	Negligible if the impurities transmit light without affecting light polarization

Table 5

Methodological comparison of specificities of the XRD, SHG and TE techniques.

Specificities	XRD	SHG	TE
Scale of observation	Entire fibre volume	Single plane	Entire fibre volume
Calculation output	1D Direct mean MFA	2D Mean value per pixel	2D Mean value per processing x-y window
X-y spatial resolution of MFA calculation	X-ray beam size along the fibre: 20 μm	1.1 μm	Depending on the processing window
Access to MFA distribution for each measurement	No	Yes (standard deviation)	No
Sign of MFAs	+	+/-	+/-
Observation of defects	**Possible**: if sufficient resolution	**Difficult**: Most defects appear as dark areas	**Difficult**: assumption of fibre wall symmetry no longer fulfilled

with the fibre in a dry state. NIS elements (NIKON, France) software was used to set the parameters of the multiphoton microscope and collect the data. The reconstruction of the entire fibre was performed on Fiji using the "stitching" plugin developed by Preibisch et al. [34]. A MATLAB script (The MathWorks, Inc., Natick, MA) using an approach developed in gager et al. [35] and adapted in Melelli et al. [16] was adjusted to evaluate the microfibril angles between -90° and 90° and plot histograms of their frequencies. The histogram of the preferred orientation of pixels was computed in three steps: applying grey level granulometry curves using linear structuring elements with orientations between -90° and 90°, summarizing the granulometry curves by computing the typical sizes in each direction and estimating the preferred orientation from the typical sizes. A mean MFA value and standard deviation representing the MFA dispersion were calculated from each resulting histogram using a Gaussian curve fitting. In order to obtain mean values comparable with XRD, the resulting image of the whole fibre was cropped into several images with the same length and spacing as in the XRD measurement, as illustrated for nettle fibre N1 in Fig. 2.

Although qualitative information is easily acquired by the direct observation of the SHG image, the data processing to obtain statistically reliable mean MFA values is tedious and greatly depends on the quality of the signal in the initial image. Examples of optimal (left) and less confident (right) data processing results are displayed in Fig. 2.

Refining the data processing by adding morphologic criteria, for instance, could be considered in future work. In the figures of the present study, the data with higher confidence are represented by filled circles and used for the future boxplots.

2.4. Transmission ellipsometry microscopy

Transmission Ellipsometry (TE) measurements were carried out using an in-house developed microrobotic system [36,37] which is equipped with an advanced polarization microscopy module. The system is intended for automated characterisation of mechanical properties of short fibres, but its polarization imaging facilities were utilized to produce MFA maps, similar to [38,39]. The crystalline microfibrils are known to exhibit birefringence which is imaged using the TE imaging scheme as discussed in [25]. The registered intensities are transformed into corresponding MFA values using mathematical formulations of polarization ellipsometry. Technically, a three-wavelength illumination,

precisely controlled polarizers, collimation and optical components for imaging, function together to capture birefringence images of different polarizations sequentially along the fibre at each wavelength. Once the fibre is mounted on the system, twelve images (at four polarizer angles (0, 45, 90 and 135°) x three wavelengths (457, 525 and 624 nm)) are captured using a camera (IDS GmbH, Germany, UI-3280CP-M-GL_Rev_2, field of view: 636 × 761 μm2, resolution: 0.31 μm/pixel) and a 10x objective lens (MY10X-803 - 10X Mitutoyo Plan Apochromat Objective). In this study. the entire fibre was imaged in 3 or 6 segments (along the 1 mm or 4 mm fibres, respectively) and reconstructed to a single image by stitching. Data processing was carried out in MATLAB R2022a by selecting the fibre region with an appropriate region of interest (ROI) and extracting the pixel intensities solely from the fibre region. TE formulations allow MFA computation from any ROIs [25]. However, to obtain mean MFAs comparable with the one from XRD, a TE scanning window of the same width and pitch of XRD was selected, as illustrated in Fig. 3. Nevertheless, a variable scanning window height (variable according to fibre diameter) was used to tackle variations in the fibre diameter. A mean MFA was computed independently for each location of the scan.

3. Results and discussion

3.1. Biochemical and geometrical characterization of fibres

The geometry and the composition of plant fibres are generally linked to their role within the plant. In the case of cotton, for instance, their aim is to promote the dissemination of the seeds by the wind, not needing strong mechanical properties. The fibres are therefore unitary, elongated and helically shaped, leading to entanglement and cocoon formation around the seeds [5]. The twist occurs upon drying of the fibres after fruit capsule opening [5,40]. Regarding biochemical composition, the high cellulose content of cotton is confirmed in this study; with a glucose content of 71.9 ± 2.8%. On the contrary, non-glucosidic monosaccharides and lignin show minor contents, which represent less than 1.5% and 1.6%, respectively. The cellulose and pectin contents are lower than the values reported by Bourmaud et al. [5], possibly due to differences in genetic, growth or processing conditions (the cotton is non-mercerized in this study) as well as differences in measurement methods, as highlighted previously in the case of flax [6].

Sisal fibres come from the leaves, which play a moderate role of structural support. They are assembled in lignified bundles with a higher porosity content, allowing for the transportation of saccharides bricks produced by photosynthesis [5]. Fig. 4 highlights the lower cellulose content (50.5 ± 1.4%) compared to cotton, and the high lignin content of 10.9 ± 0.1%. Moreover, high xylose (14.4 ± 0.3) and galacturonic acid (4.6 ± 0.2%) contents can be noticed, associated respectively to hemicelluloses and pectins. The results are in agreement with Bourmaud et al. and typical of a xylan-type fibre [5], except the lower pectin content which might originate from differences in extraction processes [41].

Finally, nettle fibres are bast fibres contributing to the stability of the stems in supporting tissues. High crystalline cellulose content and low MFA values are, therefore, expected. Depending on the variety, glucose content varies between 52.0 ± 2.8 and 62.7 ± 0.6%. High galacturonic acid content (between 6.5 ± 0.2 and 11.4 ± 0.4), associated with pectins, and low lignin content (between 2.8 ± 0.1 and 4.3 ± 0.0) are also visible in Fig. 4. Moreover, values for cellulose crystallinity have been reported between 55% and 71% for sisal [41,42], and between 58% and 69% for mature cotton [43]. Regarding nettle, values between 28% and 66% have been described, slightly lower than for flax [44]. Overall, it can be noted that cotton, nettle and sisal all appear as pertinent candidates for MFA measurements as they contain a significant level of crystalline cellulose.

The geometry of the fibres, including their outlines and internal porosities were obtained by X-ray microtomography, a widely used technique for plant fibres [7,45,46]. Qualitative illustrations are displayed in Fig. 5. The cotton fibre shows no internal porosity (referring to both the central lumen and cavities) with a ribbon-like and highly twisted structure. Regarding the two nettle fibres from the Roville variety N1 and N2, an elliptical shape is detected. N3 presents a shape closer to a circular cross-section, while N4 shows a more intricate shape, which could be explained by the presence of surface contaminants. Low porosity contents and collapsed shapes could be explained by the fibre extraction process or the drying of the fibre during the long scanning time (Table 3). Finally, the sisal fibre appears to be a double fibre instead of a unitary fibre, highlighting the difficulty of mechanical extraction of unitary fibres due to the limited length of the fibre and the lignified nature of the bundles. Similar extraction difficulty is associated with other short plant fibres possessing high lignin content such as jute or kenaf fibres, for instance. The high porosity content of the sisal fibres, attributed mainly to the central lumen, is evidenced (dark areas) in the images agreeing with their role of nutrient transportation within the plant.

3.2. Case study of nettle fibres: comparison between the methods

For the three techniques used to determine MFA, the fibres were characterized at a moisture content that was equilibrated with the testing ambient conditions. The latter might have varied slightly depending on the considered method but remained, in any case, in the range of 19–21 °C for the temperature and 30–50% for the RH. It is well established in literature that even if cellulose does not absorb moisture within its crystalline structure, the moisture absorption in the cell wall induces changes and deformation in the cellulose crystals [47,48]. Despite these deformations in the cellulose crystals, no significant influence of moisture has been observed in the MFA of plant fibres, except in the dislocations area [49].

It is also true that tensile loading can induce some realignment of cellulose microfibrils but this mechanism is partially reversible and the tensile forces applied during the pre-stretching/aligning were very low and may induce only very slight changes in MFA.

MFA measurements using the three considered techniques were obtained for nettle fibres N1 to N4 (Fig. 6 to Fig. 9). While XRD only provides positive values, both positive and negative MFA are obtained by SHG and TE (Fig. 6a to Fig. 9a). For TE, the sign is governed by the

macrofibril orientation in the front wall. A change of sign might therefore indicate a change of front wall and back wall orientations (based on the assumption of the fibre wall symmetry), likely caused by a twist of the fibre. Some couplings between moisture sorption, mechanical loading and twisting have been observed in the literature for plant fibres [50]. Considering the slight variation in RH and the low tensile force applied during MFA measurements in our study, MFA variations cauded by these factors are supposed to be very small. In the case of nettle fibres N1 to N4, values are mainly negative, indicating a lower level of twist which is confirmed by μ-CT. In the SHG measurements, the values are mainly negative, and based on a direct single plane observation. The change of sign along the fibre indicates a change of macrofibril preferential orientation, as illustrated in the images 1 and 2 of Fig. 7. As mentioned in the material and method description, some positive values might also arise from initial images with no visible macrofibrils, which creates artefacts during MATLAB processing. This results in a low confidence in MFA values which is illustrated using empty circles in the following figures.

In order to better compare the measurements between the techniques, the absolute MFA values along each fibre are represented in Fig. 6e to Fig. 9e and summarized using boxplots in Fig. 10. For all nettle fibres, SHG provides lower levels of MFA compared to TE and XRD, with median values between 1° and 2° XRD and TE show higher median values contained within 5° and 13° The scale of observation is an important feature which might explain the differences of MFAs reported along the fibres. XRD and TE provide only averaged MFA orientations over the whole fibre volume, while SHG allows a direct observation of the macrofibrils and their orientation in a given plane. The median MFA values obtained with XRD and TE are close to each other, except for N2. As presented in [37], the accuracy of the TE based MFA mapping is remarkably high for fibres with high MFAs. However, for fibres with low MFAs (-10° to +10°) such as nettle, high measurement accuracy requires a very precise control over the background light uniformity, alignment of optical components and the fibre axis.

In addition, XRD provides a lower MFA variability along the fibres than SHG and TE, as evidenced in Fig. 10 by the smaller length of the boxplots. It is likely to be due to the size of the X-ray beam: in XRD the MFA measurements are averaged along the width of a 20 μm measurement window. For future experiments, the use of a microbeam will help obtain a higher spatial resolution and a better capture of the MFA heterogeneities along plant fibres [21]. For TE, the MFA absolute values are comprised between 0 and 18°, indicating a higher variability along the fibres. Finally, SHG presents absolute MFAs comprised between 0 and 7° These variations are linked to the direct observation of macrofibrils in a single plane (the S2 layer is usually preferred), as evidenced in Fig. 7 (1. and 2.).

Regarding the link between MFA and defects, it has to be mentioned that the plant fibres chosen within this study do not contain, arguably, as many defects as other plant fibres such as those reported for flax or hemp, due to mechanical extraction processes that can be more severe. However, a possible correlation between the defects and resulting MFA is investigated for a fibre containing visible defects, which appear as bright areas under polarized light in Fig. 8c. As illustrated, it is difficult to link the defects to the resulting MFA peaks (Fig. 8a and e). In SHG measurements, the defects might lead to a disorganization of the microfibril network that consequently cannot provide SHG signal, since it occurs only under certain conditions such as a well-ordered structure, complicating the observation of the microfibrils (Fig. 7-/, Fig. 8-) [51]. Therefore, it induces uncertainties in the mean calculated MFA. Adding water to the fibres can help to partially overcome the problem but it is not a suitable approach in our study, since we aim to compare the results with the other techniques performed in a dry state. Moreover, the most severe defects might result in a misalignment of the entire fibre which is difficult to distinguish from an internal macrofibril disruption. In the case of N3, the waviness of the fibre visible in Fig. 8b, c and d is also a source of error that has to be taken into account [52]. Depending on the

geometry of the fibre and the observation plane, zones of poor focus might appear as highlighted in (Fig. 8-), leading to uncertainties.

For TE, variations of MFA are observed along the fibres, but again the link with the defects is difficult to assess. Moreover, the defect severity might be different between the front wall and the back wall, inducing uncertainties as the fibre wall symmetry assumption is no longer fulfilled.

In XRD measurements, the length of the X-ray beam is a limiting factor to obtain local information of the MFA heterogeneities within the cell walls. Additionally, another limiting factor in the XRD scanning is to determine the exact location of MFA measurements on the optical images along the fibre. The observation of more severely defected fibres such as flax or hemp could be of interest for further investigations.

The effect of surface impurities on the MFA measurements is illustrated in the right image in Fig. 9, polluting the images for SHG, and inhibiting the observation of defects by polarized light microscopy. As the surface impurities are likely to be amorphous remains of the middle lamella (i.e. lignin and non-cellulosic polysaccharides) connecting fibres to their neighbours [6], it should not influence the XRD measurements, which are based on the diffraction of crystalline cellulose. In the case of TE, the surface impurities are smaller in size than the scanning area. If they are not autofluorescent or able to transmit light without affecting polarization, their effects can be ignored.

3.3. Case study of sisal and cotton fibres: highlighting the limits of the methods

The MFA values obtained along cotton and sisal fibres are displayed in Figs. 11 and 12. Unfortunately, in the case of XRD, neither cotton nor sisal unitary fibres gave enough signal intensity to estimate the MFA. As both plant fibres contain a sufficient amount of crystalline cellulose (Fig. 4) and cellulose signal was successfully observed on a batch of several cotton fibres positioned alongside each other, their small diameter might be an explanation: not enough crystallites fulfil Bragg's law with these experimental parameters if only a single unitary fibre is tested. For future experiments, a change of experimental parameters could be considered, as measurements along cotton unitary fibres have already been described in literature using an X-ray microbeam [53].

In the TE measurement, the MFAs obtained for cotton are higher than for nettle, being between -16° and +20°, in agreement with values found in literature [5,10,16]. In Fig. 11, the repeated cotton twisting might explain the change-over between positive and negative MFAs while the deviation of the fibre axis from a horizontal alignment increases uncertainty in the determination of the MFA value. Thus, in TE, the fibre axis orientation directly affects the reliability of MFA measurements.

In the case of SHG, mean MFA values between -8° and +10° are reported in Fig. 11. In some areas such as the magnified view in Fig. 11e, direct observation gives MFA between 20° and 25°, in agreement with the literature [5,10,16]. However, the quantitative analysis of MFA is hindered by brightness and geometrical issues linked to the twisted configuration of the fibres. Indeed, in other areas the macrofibril network is not visible or the twist induces both positive and negative MFAs as highlighted in Fig. 11d, decreasing the mean MFA. Moreover, the strength of the SHG measurements lies in its plane selective imaging modality. In the case of cotton, it should allow the observation of the orientation changes depending on the observed sublayer. But as mentioned by Melelli et al. [15], different layers might be involved in the same plane of observation due to the twisting structure of cotton, complicating the interpretation. No macrofibrils could be observed at the "nodes" of the twist, which appear as darker areas. Finally, the changes of fibre orientation induced by the twist, introduce errors in the MFA calculation for all techniques that should be further considered.

Regarding sisal, it appears that the sisal fibre was in fact composed of two unitary fibres as two lumens can be distinguished (Fig. 5). Indeed, depending on the fibre dimensions and composition, some fibres are easier to separate than others. In addition to sisal, all short fibres with high lignin content are difficult to extract mechanically. If the fibres are placed above each other (instead of along each other), the assumption of fibre wall symmetry upon which is based the TE theory is not fulfilled anymore, inducing uncertainties. In the SHG image, a single lumen is highlighted by the white arrow to the left (Fig. 12c), favouring the "fibre above fibre" configuration. Moreover, the macrofibril network was difficult to identify in the case of sisal observed by SHG, possibly due to geometrical effects (thinner walls due to high porosity content for instance). On the magnified view obtained by SHG (Fig. 12d), a possible pattern hypothetically attributed to the macrofibril network provides manually values around 20°, in agreement with the literature. However, the mean values obtained with the quantitative method developed (Fig. 12a) do not reflect the direct observation and highlight the limit of this method for sisal fibres.

3.4. Summary of comparison between SHG, TE and XRD

A summary of the discussions highlighting the sources of uncertainty and specificities of each technique to measure MFAs along plant fibres is presented in Table 4 and 5, respectively.

Regarding possible damage of the sample for each technique, we believe that TE and SHG are not detrimental, but we cannot exclude any damaging effects related to the X-ray beam. It is for this reason, that all experiments were performed in the same order for all fibres, to systematically produce the same impact, if any.

Regarding XRD, low mechanical properties were observed in a previous study [54], confirming a possible damage of the fibres upon X-ray measurement. However, no significant differences between the samples scanned with different X-ray beam sizes and resulting acquisition times were evidenced here.

4. Conclusions

Second Harmonic Generation (SHG), Transmission Ellipsometry (TE) and X-ray Diffraction (XRD) were used to estimate microfibril angle (MFA) along nettle, cotton and sisal fibres, revealing the respective characteristics, strengths and weaknesses of these three non-destructive methods. On the four tested nettle unitary fibres, lower MFA levels are reported by SHG (median values between 1° and 2°) than by XRD and TE (median values between 5° and 13°). This can be attributed to the difference in measured sample volume. Indeed, the mean MFA value obtained with SHG, is acquired from a single observation plane chosen in the S2 layer, which is the thickest in the fibre. However, as XRD and TE measurements are made over both the front and the back walls of the fibre, the measured volume is thus different between the methods. The MFA variations along the fibres are higher for SHG and TE than for XRD, probably due to the low resolution linked to the 20-μm-length of the X-ray beam size. Regarding SHG, reliable and quantitative data are dependant on the primary image quality while the current processing routine could be further improved. However, the technique still provides high quality qualitative information with a direct visualization of the cellulose macrofibrils in nettle. Moreover, valuable information about the MFA distribution can be obtained from each picture, revealing the heterogeneity of the macrofibril orientations within a single observation plane. In comparison, the reduced magnification and reduced optical resolution due to low NA (SHG objective lens: 16x, 0.8 NA; TE objective lens: 10x, 0.28 NA) can be a limiting factor in direct qualitative observations with TE.

Regarding the defect observation, XRD appears as the most promising measurement method provided that such an X-ray μ-beam is used, which helps to obtain enough signal intensity for smaller diameter fibres such as the cotton and the sisal used in the present study. In SHG measurements, the defects result in a higher uncertainty in MFA measurements, due to destructive interferences. For the TE method, although the light polarization features help to address defect observation, the deviation from fibre wall symmetry assumption prevents the

detection of defects from the MFA measurements. In future work, plant fibres containing more defects such as flax or hemp could be considered for deeper investigations.

Surface impurities seem to interfere with the MFA measurements especially with SHG and should therefore not be preferred when investigating contaminated fibres with remaining cortical tissues in a dry state. The addition of water to fibres could also be considered in further experiments to improve the SHG signal.

For cotton fibres, higher MFAs were reported by TE measurements, with values between -16° and 20° The high twisting levels observed induce a change of sign as well as uncertainties in the output, especially in the SHG measurement where only qualitative direct MFA measurements appear in agreement with literature. Regarding sisal, the macrofibrils were difficult to distinguish by direct observation with SHG and the double fibre configuration revealed by μ-CT weakens the reliability of the TE measurements.

Finally, the fibre alignment and the fibre geometry are the key parameters that should be carefully characterized and considered in the MFA calculations in the future, as they induce uncertainties for all techniques.

Funding

Declaration of Competing Interest

The authors declare that they have no known competing financial interests or personal relationships with other people or organizations that could have appeared to influence the work reported in this paper.

Data availability

Data will be made available on request.

Acknowledgments

References

[1] A. Partanen, M. Carus, Biokomposite: überzeugende Lösungen aus Erneuerbaren Materialien, Nova-Institute, 2020.
[2] C. Baley, Analysis of the flax fibres tensile behaviour and analysis of the tensile stiffness increase, Compos. Part A: Appl. Sci. Manuf. 33 (2002) 939–948.
[3] Barnett, J.R. and V.A. Bonham, Cellulose microfibril angle in the cell wall of wood fibres. 2004. 79(2): p. 461–472.
[4] L. Donaldson, Cellulose microfibril aggregates and their size variation with cell wall type, Wood Sci. Technol. 41 (5) (2007) 443–460.
[5] A. Bourmaud, et al., Towards the design of high-performance plant fibre composites, Prog. Mater. Sci. 97 (2018) 347–408.
[6] E. Richely, et al., A critical review of the ultrastructure, mechanics and modelling of flax fibres and their defects, Prog. Mater. Sci. 124 (100851) (2021) 1–31.

[7] A. Bourmaud, et al., Elucidating the formation of structural defects in flax fibres through synchrotron X-ray phase-contrast microtomography, Ind. Crops Prod. (2022) 184.
[8] L. Kozlova, et al., On the origin of bast fiber dislocations in flax, Ind. Crops Prod. (2022) 176.
[9] A. Hernandez-Estrada, J. Müssig, M. Hughes, The impact of fibre processing on the mechanical properties of epoxy matrix composites and wood-based particleboard reinforced with hemp (Cannabis sativa L.) fibre, J. Mater. Sci. (2022).
[10] D.B. Anderson, T. Kerr, Growth and structure of cotton fiber, Ind. Eng. Chem. 30 (1) (1938) 48–54.
[11] C.W. Hock, Microscopic structure of flax and related bast fibers, J. Res. Natl. Bur. Stand. (1934) (1942) RP1482.
[12] H.H. Wang, et al., An improved fibril angle measurement method for wood fibres, Wood Sci. Technol. 34 (2001) 493–503.
[13] C. Wang, et al., Investigation of microfibril angle of flax fibers using X-ray diffraction and scanning electron microscopy, J. Nat. Fibers 17 (7) (2018) 1001–1010.
[14] A. Hernandez-Estrada, M. Reza, M. Hughes, The structure of dislocations in Hemp (Cannabis sativa L.) fibres and implications for mechanical behaviour, Bioresources 15 (2020) 2579–2595.
[15] J.-.C. Roland, M. Mosiniak, D. Roland, Dynamique du positionnement de la cellulose dans les parois des fibres textiles du lin (Linum usitatissimum), Acta Botanica Gallica 142 (5) (1995) 463–484.
[16] A. Melelli, et al., Microfibril angle of elementary flax fibres investigated with polarised second harmonic generation microscopy, Ind. Crops Prod. 156 (112847) (2020) 1–10.
[17] R.M. Brown, A.C. Millard, P.J. Campagnola, Macromolecular structure of cellulose studied by second-harmonic generation imaging microscopy, Optic. Lett. 28 (22) (2003) 2207–2209.
[18] L.A. Donaldson, Microfibril angle: measurement, variation and relationships – a review, Iawa J. 29 (2008) 345–386.
[19] M.-.P. Sarén, R. Serimaa, Determination of microfibril angle distribution by X-ray diffraction, Wood Sci. Technol. 40 (6) (2005) 445–460.
[20] M. Müller, et al., Combined X–ray microbeam small–angle scattering and fibre diffraction experiments on single native cellulose fibres, J. Appl. Crystallogr. 33 (2000) 817–819.
[21] K. Kölln, et al., Mechanical properties of cellulose fibres and wood. Orientational aspects in situ investigated with synchrotron radiation, J. Synchrotron Radiat. 12 (2005) 739–744.
[22] D.H. Page, A method for determining the fibrillar angle in wood tracheids, J. Microsc. 90 (1969) 137–143.
[23] R.D. Preston, The organization of the cell wall of the conifer tracheid. Philosophical transactions od the royal society of London, Series B, Biol. Sci. 224 (511) (1934) 131–174.
[24] M. Sedighi-Gilani, H. Sunderland, P. Navi, Microfibril angle non-uniformities within normal and compression wood tracheids, Wood Sci. Technol. 39 (6) (2005) 419–430.
[25] C. Ye, M.O. Sundström, K. Remes, Microscopic transmission ellipsometry: measurement of the fibril angle and the relative phase retardation of single, intact wood pulp fibers, Appl. Opt. 34 (28) (1994) 6626–6637.
[26] L.G. Thygesen, N. Gierlinger, The molecular structure within dislocations in Cannabis sativa fibres studied by polarised Raman microspectroscopy, J. Struct. Biol. 182 (3) (2013) 219–225.
[27] L.G. Thygesen, P. Hoffmeyer, Image analysis for the quantification of dislocations in hemp fibres, Ind. Crops Prod. 21 (2) (2005) 173–184.
[28] C. Hoebler, et al., Rapid acid-hydrolysis of plant-cell wall polysaccharides and simplified quantitative-determination of their neutral monosaccharides by gas-liquid chromatography, J. Agric. Food Chem. (1989) 37.
[29] Lahaye, M., M., et al., Cellulose, pectin and water in cell walls determine apple flesh viscoelastic mechanical properties. 2020. 232: p. 115768.
[30] A.B. Blakeney, et al., A simple and rapid preparation of alditol acetates for monosaccharide analysis, Carbohydr. Res. 113 (1983) 291–299.
[31] J.F. Thibault, Automatisation du dosage des substances pectiques par la methode au meta-hydroxydiphenyl. Lebensmittel - Wissenschaft + Technologie, Food Sci. + Technol. 12 (5) (1979) 247–251.
[32] R. Hatfield, R.S. Fukushima, Can Lignin Be accurately measured? Crop Sci. 45 (3) (2005) 832–839.
[33] E. Richely, et al., Influence of defects on the tensile behaviour of flax fibres: cellulose microfibrils evolution by synchrotron X-ray diffraction and finite element modelling, Compos. Part C: Open Access (2022).
[34] S. Preibisch, S. Saalfeld, P. Tomancak, Globally optimal stitching of tiled 3D microscopic image acquisitions, Bioinformatics 25 (11) (2009) 1463–1465.
[35] V. Gager, et al., Oriented granulometry to quantify fibre orientation distributions in synthetic and plant fibre composite preforms, Ind. Crops Prod. (2020) 152.
[36] Zarei, A., D. Kattipparambil Rajan, and P. Kallio, Slippage prediction in microrobotic fiber characterization. 2022.
[37] al., Z.A.e., A microrobotic platform for efficient microfibril angle measurements with tensile characterisation. 2022.
[38] J. Hirvonen, et al., Semi-automatic measurement of microfibril angle on a microrobotic platform, in: 2014 International Conference on Manipulation, Manufacturing and Measurement on the Nanoscale (3M-NANO), 2014, pp. 326–329.
[39] P. Saketi, et al., A flexible microrobotic platform for handling microscale specimens of fibrous materials for microscopic studies, J. Microsc. 248 (2) (2012) 163–171.
[40] J.E. Van Dam, T. Gorshkova, Encyclopedia of applied plant sciences, Encyclopedia of Appl. Plant Sci. (2003).

[41] J. Müssig, Industrial Applications of Natural fibres: Structure, Properties and Technical Applications. Renewable Resources, Wiley, 2010, p. 538.

[42] A. El Oudiani, et al., Crystalline Character of Agave americana L. Fibers, Textile Res. J. 78 (7) (2008) 631–644.

[43] X.-.P. Hu, Y.-.L. Hsieh, Crystalline structure of developing cotton fibers, J. Polym. Sci.: Part B Polym. Phys. 34 (1996) 1451–1459.

[44] M. Viljanen, J.A. Suomela, K. Svedström, Wide-angle X-ray scattering studies on contemporary and ancient bast fibres used in textiles – ultrastructural studies on stinging nettle, Cellulose 29 (4) (2022) 2645–2661.

[45] J. Beaugrand, S. Guessasma, J.E. Maigret, Damage mechanisms in defected natural fibers, Sci. Reports, 7 (1) (2017) 14041.

[46] E. Richely, et al., Novel insight into the intricate shape of flax fibre lumen, Fibers 9 (4) (2021).

[47] K. Abe, H. Yamamoto, Mechanical interaction between cellulose microfibril and matrix substance in wood cell wall determined by X-ray diffraction, J. Wood Sci. 51 (4) (2005) 334–338.

[48] S. Zabler, et al., Moisture changes in the plant cell wall force cellulose crystallites to deform, J. Struct. Biol. 171 (2) (2010) 133–141.

[49] L. Nuez, et al., Exploring the effect of relative humidity on dynamic evolution of flax fibre's microfibril angle through in situ tensile tests under synchrotron X-ray diffraction, Ind. Crops Prod. 188 (2022) 115592.

[50] V. Placet, O. Cisse, M.L. Boubakar, Influence of environmental relative humidity on the tensile and rotational behaviour of hemp fibres, J. Mater. Sci. 47 (7) (2012) 3435–3446.

[51] A. Melelli, et al., Extensive investigation of the ultrastructure of kink-bands in flax fibres, Ind. Crops Prod. 164 (2021).

[52] O. Paris, M. Müller, Scanning X-ray microdiffraction of complex materials: diffraction geometry considerations, Nuclear Instruments and Methods in Phys. Res. B 200 (2003) 390–396.

[53] M. Müller, et al., Identification of ancient textile fibres from Khirbet Qumran caves using synchrotron radiation microbeam diffraction, Spectrochimica Acta Part B: Atomic Spectroscopy 59 (10–11) (2004) 1669–1674.

[54] E. Richely, et al., Influence of defects on the tensile behaviour of flax fibres: cellulose microfibrils evolution by synchrotron X-ray diffraction and finite element modelling, Compos. Part C: Open Access 9 (2022), 100300.

[55] Stevanic, J.S. and L. Salmén, Orientation of the wood polymers in the cell wall of spruce wood fibres. 2009. 63(5): p. 497–503.

[56] I.D. Cave, Theory of X-ray measurement of microfibril angle in wood, Part 1. The condition for reflection X-ray diffraction by materials with fibre type symmetry, Wood Sci. Technol. 31 (1997) 143–152.